J Neurophysiol 104: 2375–2388, 2010.
First published September 1, 2010; doi:10.1152/jn.00089.2010.

Sensory-Spatial Transformations in the Left Posterior Parietal Cortex May Contribute to Reach Timing

Elizabeth B. Torres,[1] Anastasia Raymer,[2] Leslie J. Gonzalez Rothi,[3] Kenneth M. Heilman,[3] and Howard Poizner[4]

[1]*Psychology Department, Rutgers University, Piscataway, New Jersey;* [2]*Department of Veterans Affairs, Early Childhood Special Education & Special Education, Child Study Center, Old Dominion University, Norfolk, Virginia;* [3]*Department of Neurology, McKnight Brain Institute, Gainesville, Florida; and* [4]*Institute for Neural Computation, University of California, La Jolla, California*

Submitted 20 January 2010; accepted in final form 27 August 2010

Torres EB, Raymer A, Gonzalez Rothi LJ, Heilman KM, Poizner H. Sensory-spatial transformations in the left posterior parietal cortex may contribute to reach timing. *J Neurophysiol* 104: 2375–2388, 2010. First published September 1, 2010; doi:10.1152/jn.00089.2010. The posterior parietal cortex (PPC) contains viewer-centered spatial maps important for reaching movements. It is known that spatial reaching deficits emerge when this region is damaged, yet less is known about temporal deficits that may also emerge because of a failure in sensory-spatial transformations. This work introduces a new geometric measure to quantify multimodal sensory transformation and integration deficits affecting the tempo of reaching trajectories that are induced by injury to the left PPC. Erratic rates of positional change involving faulty maps from rotational angular displacements to translational linear displacements contributed to temporal abnormalities in the reach. Such disruptions were quantified with a time-invariant geometric measure. This measure, paired with an experimental paradigm that manipulated the source of visual guidance for reaches, was used to compare the performance of normal controls to those from a patient (T.R.) who had a lesion in his left-PPC. For controls, the source of visual guidance significantly scaled the tempo of target-directed reaches but did not change the geometric measure. This was not the case in patient T.R., who altered this measure. With continuous, extrapersonal visual feedback of the target, however, these abnormalities improved. Vision of the target rather than vision of his moving hand also improved his arm-joint rotations for posture control. These results show that the left PPC is critically important for visuo-motor transformations that specifically rely on extrapersonal cues to align rotational-arm and linear-hand displacements and to continuously integrate their rates of change. The intactness of this system contributes to the fluidity of the reach's tempo.

INTRODUCTION

In our daily activities, we often perform reaching motions that are partly guided by vision, at least during some portions of the movement. For example, when we reach for a nearby cup of coffee while reading an interesting article in the newspaper, we can briefly gaze at the cup and return to reading while our hand reaches to the remembered spatial location of this cup. In this situation, most likely once the target of our reach is visualized, a motor plan that is partly monitored with proprioceptive feedback is developed to move and guide the hand so that it accurately reaches the target. Occasionally, we might miss the cup, gaze at its relation to the hand and correct the reach. The posterior parietal cortex (PPC) is important in these visuomotor computations, requiring estimation of eye-hand-target distance (Buneo et al. 2002), as well as the conversion of visual information into a movement vector used to guide the hand toward the final target. This region of cortex is also involved in coordinate transformations mapping visual-spatial goals to changes in body configurations to attain those goals. Accurate reaching requires that visual-retinotopic information has to be altered into a body-based representation (Andersen and Zipser 1988; Zipser and Andersen 1988). Less explored, however, is the potential contribution of sensory input and sensory-spatial transformations in the PPC to the stability of the overall motion tempo. In particular, we do not know how the rates of change of displacements of different orders and their inter-relations may be affected in normal participants when their source of visual guidance switches between the external target and the moving hand. This kind of interplay often occurs when we intentionally try to help correct our reaching errors. Does the source of visual guidance affect the relative scales of acceleration and speed in reaching movements? How is the movement timing affected?

The control and coordination of movement timing is thought to arise from motor-related regions including the basal ganglia and the cerebellum, as suggested by their disruption (Schmahmann 2004; Schmahmann et al. 2007). These are aspects of the timing emerging from a sort of "ticking clock" dictating the moment to moment temporal dynamics in automated behavior (Fujii and Graybiel 2005; Jin et al. 2009). Another contributing factor to the motion's tempo that seems different from the timing control refers to the relative scaling of acceleration and speed at fixed lengths of time. These kinematics aspects of the reach are tied to time-invariant sensory-spatial transformations involving different frames of reference (Buneo et al. 2008) and thought to recruit areas of the PPC (Andersen and Zipser 1988; Zipser and Andersen 1988).

Research addressing the dissociation between kinematics and dynamics in goal-oriented motions has provided more evidence in area 5 of the PPC for the computation of movement kinematics than movement dynamics (Kalaska and Hyde 1985; Kalaska et al. 1990, 1997a). Furthermore, manipulations of sensory information have separated kinematics-based from dynamics-based learning (Krakauer et al. 1999) and defined important distinctions in the on-line control of reaching motions regarding the roles of motor and parietal regions (Desmurget and Grafton 2000). It is an open question how the disruption of the PPC may impact time-invariant sensory-

Address for reprint requests and other correspondence: E. B. Torres, Psychology Dept., Rutgers University (Busch Campus), 152 Frelinghuysen Rd., Piscataway, NJ 08854 (E-mail: ebtorres@rci.rutgers.edu).

Downloaded from journals.physiology.org/journal/jn (073.194.068.111) on October 11, 2020.

spatial transformations underlying the kinematics variables that may also affect the fluidity of the reach tempo.

Intact sensory-spatial transformations seem necessary to achieve comparable displacements in different sensory spaces (Fig. 1) and to align sensory transduction occurring at different time scales. In a biological system, the correct alignment and sensing of rotational displacements of the arm's joints ought to be critical to produce, in unique correspondence, smooth rates of rotational and positional displacements at the end effector. We surmised here that this correspondence must be continuously preserved under sensory-spatial transformations to ensure the fluidity of the motion trajectories.

Because of the redundant degrees of freedom in the arm, and the inherent nonlinearity between rotations and translations (Fig. 1, *A* and *B*), large rotational displacements at the arm joints may produce incongruent or no translation of the hand. Likewise, the hand may abruptly accelerate at step n and faulty sensory processing may prevent the arm from properly rotating at step $n + 1$ to compensate for the sudden change in hand position. The type of chronological information proposed here to be contributed by the parietal system emerges from sensory-spatial transformations. Such transformations are necessary to correctly align positional displacements from angular rotations and linear translations to make them comparable (Fig. 1*C*) and to produce a fluid reach tempo.

Somehow the primate arm system maintains a time-invariant linear relation between arm joint rotations and changes in hand configuration (Torres and Zipser 2004) as noted in earlier studies of pointing motions (Atkeson and Hollerbach 1985; Nishikawa et al. 1999; Soechting 1988; Soechting and Lacquaniti 1981). Such studies have shown that neither loads nor instructed changes in speed significantly alter the linear path of the hand to targets in space. How are these kinds of time invariant linear relations of the motion trajectories affected when the posterior parietal lobe is injured? Is there any way to compensate for deficits with some form of sensory guidance?

There are many reports of movement disorders caused by PPC damage. These disorders involve mainly spatial and abstract relations, but some body-schema alterations may also emerge (Heilman and Watson 1977). The PPC has been implicated in the intentional plans of goal-directed reaches (Andersen 1995; Andersen et al. 1993), but we also know that the area 5 is sensitive to changes in arm posture (Scott et al. 1997) and less sensitive to changes in arm dynamics than the primary motor cortex (Kalaska and Hyde 1985; Kalaska et al.

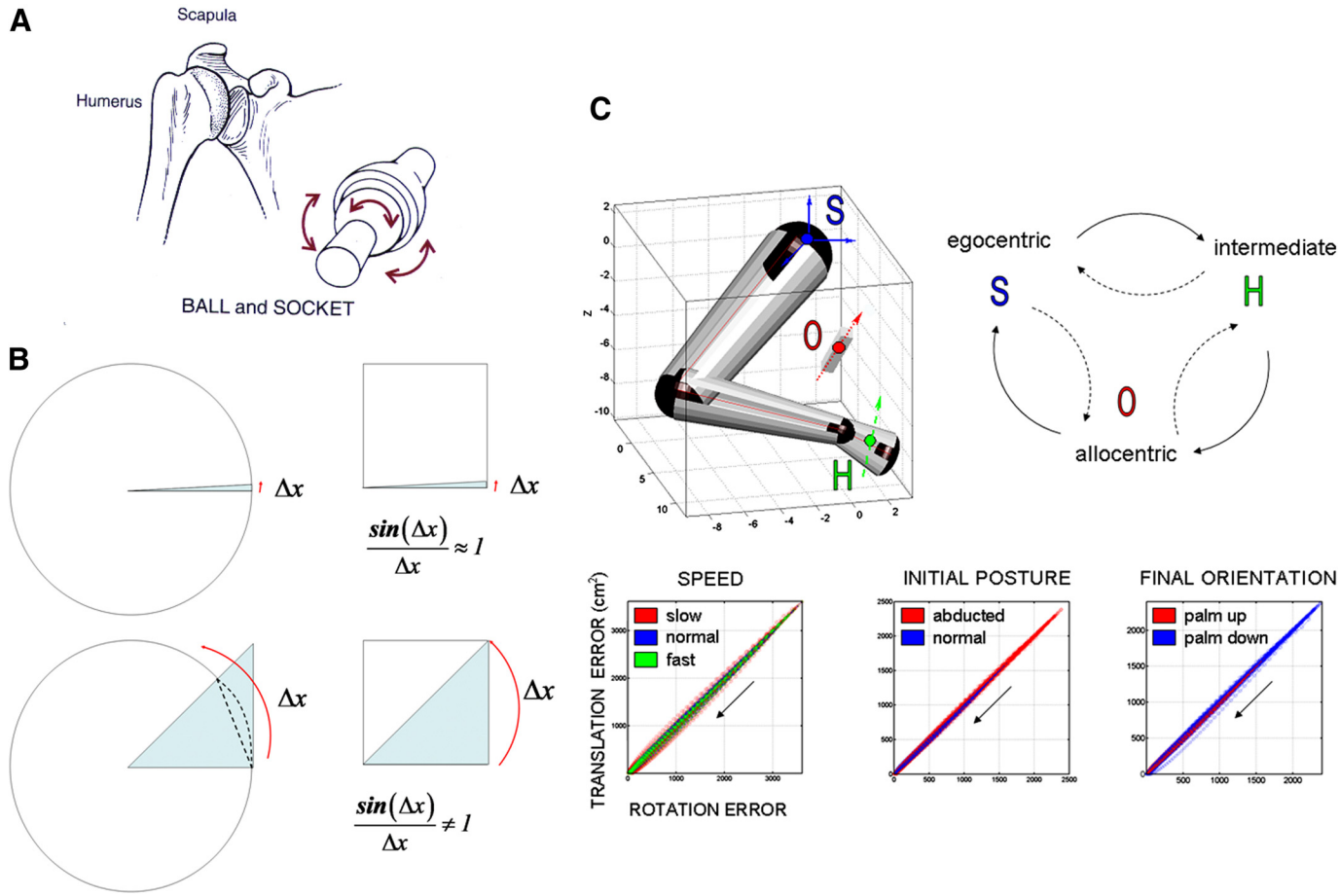

FIG. 1. The problem of comparable displacements, their transformation map and the time-invariant nature of the hand path solutions to the reaching task. *A*: ball-and-socket-rotational joint similar to that at the shoulder. *B*: for very small displacements, angular rotations and linear translations are congruent. They add up and commute (Altmann 1986). For larger displacements, their ratio diverges from unity. This property holds independent of whether such a displacement takes 1 ms or 10 s to complete, and its time-invariant solution for a redundant arm system can be equivalently obtained from different perspectives (shoulder-, hand-, object-, eye-based, etc.). *C*: humans have arms with several joints that normally co-articulate and translate the hand along linear displacement paths independent of speed, instructed initial postural configuration or instructed final orientation. This linear solution stands despite the aforementioned problem of displacement disparity and their inherently nonlinear map (taken from Torres and Zipser 2004).

Downloaded from journals.physiology.org/journal/jn (073.194.068.111) on October 11, 2020.

1990, 1997b). Its damage has been associated with various forms of spatial neglect (Heilman and Watson 1977), ideomotor apraxias (Heilman and Valenstein 2003; Poizner 1990, 1995), endpoint accuracy deficits, and problems with on-line control (Blangero et al. 2008; Desmurget et al. 1999; Grea et al. 2002; Khan et al. 2005, 2007; Pisella et al. 2000, 2009). There have been, however, no studies on the effects that faulty sensory-spatial transformations after PPC damage may have on the motion tempo, despite the known role of this region in coordinate transformations (Andersen and Zipser 1988; Zipser and Andersen 1988).

Multiple lines of evidence suggest that regions in the left hemisphere play a greater role than those in the right hemisphere in relation to movement timing (Poizner et al. 1998; Sainburg and Kalakanis 2000; Schaefer et al. 2009). The particular patient that we present here is a rare one in that he had a focal lesion of the left PPC, without damage to the motor cortex, premotor cortex, corticospinal projections, or basal ganglia. This patient also had (right) hemispatial neglect. The latter deficit occurs only in ~1 of 10 cases of left parietal lobe damage (Heilman and Valenstein 2003; Heilman et al. 1977). This case study allowed us to examine the effects of spatial neglect on deficits related to the chronological structure of the reach. Although a larger population of left PPC–injured patients would have enabled us to provide a more general conclusion, the examination of this case study will be useful to assess potential sensory transformation and integration deficits, as well as potential ways to compensate for such deficits. Indeed, unique case studies have had a striking history of success in neurology, initiating new domains of study and understanding (Heilman 2004).

The first part of this study found support for the hypothesis that the source of sensory guidance normally changed the tempo of the reach. These were scaling changes that preserved the overall temporal structure. The second part of this study compared the normal performance to the performance of a patient with left PPC damage. We asked whether, in this patient, sensory-spatial transformation deficits significantly altered the reach tempo and if a particular source of sensory guidance could compensate for such deficits. We used a time-invariant metric of sensory-spatial transformations to objectively quantify both the deficits and the improvements. We found that in this patient external guidance compensated best for sensory-spatial transformations and that such improvements contributed to regain the fluidity of the reach tempo.

METHODS

Participants

We asked *patient T.R.* and nine age-matched healthy subjects to perform three-dimensional (3D) pointing motions (forward and back to the starting point) in a dark room. *Patient T.R.* was a 62-yr-old right-handed man who sought medical attention for a severe headache 1 month before our testing. He complained of no other motor, sensory, or cognitive impairments and he could reach on command.

An examination showed no motor weakness and no primary sensory deficits. A sagittal T1 MRI scan and a transverse T2 proton-weighted axial scan completed 3 wk before testing showed a wedge-shaped area of decreased attenuation in the left posterior parietal temporal region that also involved the anterior convexity of the occipital region. These MRI findings suggest that this lesion was caused by a cerebral infarction. This lesion probably involves Brodmann's area 39 (angular gyrus), the superior part of area 37, and the lateral part of area 19 (see Fig. 1*A*).

Examination 1 mo after the onset of his symptoms showed no aphasia (Kertesz 1982), no impairments of vision or object processing (Riddoch and Humphreys 1993), and no sensory or motor deficits. He was impaired in tests of visual perception that required him to make judgments regarding the spatial orientation of visual stimuli. In the line bisection test for spatial neglect, he showed neglect of contralesional right space. We could not assess reading abilities because *patient T.R.* reported that he had developmental dyslexia and dysgraphia. He used his dominant right arm during testing because his left arm had a shunt.

Apparatus and procedures

Three conditions were designed to examine the contributions of extrapersonal versus body-centered visual cues to the initiation of reach trajectories and to their endpoints. In each of the three conditions, targets were presented as points of light within 3D space in a completely darkened room. Hand locations were in one block marked by an additional point of light on the endpoint (index fingertip), whereas in other blocks, they were not marked. The conditions differed on whether the target light remained illuminated during movement and whether the additional light on the endpoint (index fingertip) was illuminated.

In the first condition, dark, the target was extinguished before movement onset and the endpoint was not illuminated, so that movements were made in complete darkness. In the second condition, finger, the target was similarly extinguished before the movement onset, but the finger tip was illuminated throughout, thus providing a body-centered cue. In the third condition, target, the target light remained visible during the movement, providing an extrapersonal cue, but the fingertip was not illuminated.

The participants were seated with their right arm flexed at the elbow joint, forearm being semipronated and vertical such that the hand was positioned in a sagittal plane that was ~10 cm to the right of the subject's ear. (Fig. 2*B*). The subjects faced a programmable robot arm (CRS 255A, Hudson Robotics), which presented the target in 3D space. A small light-emitting diode (LED) was attached to the tip of the robot's arm and served as the target. Two optoelectronic cameras (Northern Digital) were used to record positions of five infrared emitting diodes (IREDs) that were affixed to the following segments of the subject's limb: the acromial process of the scapula (shoulder), the lateral epicondyle of the humerus (elbow), the ulnar styloid process (wrist), and the nail of the index fingertip and on the robot arm tip. The subjects were asked to fully extend their right index finger and not to move it with respect to the wrist. 2D coordinates of the IREDs were monitored by each camera. Data from both cameras were sampled at 100 Hz and stored as 2D binary files. This positioning of the subject relative to the target space prevented the subject from having to fully extend the arm to reach any target (Fig. 2*C*).

All participants attempted to "touch" the LED target with the forefinger of their right dominant arm and return their arms to their initial positions in one smooth movement. The targets were presented in a dark room. Three visual feedback conditions were used in this experiment (Fig. 2*C*).

1) Dark (no vision). The robot arm held the target for 1.5 s, after which a short auditory signal (tone) instructed the subjects to close their eyes, and the robot arm retracted. A second auditory tone 1 s later signaled subjects to "touch" the location where the target was previously displayed with their right forefinger and to bring their arm back to the initial position in smooth continuous movements without "corrections" near the target. The subjects' eyes remained closed throughout this movement.

2) Finger (vision of finger). The target LED went off just before the signal to move, but the LED on the fingertip remained on throughout the movement and the participant's eyes remained open during the reaching movement.

Downloaded from journals.physiology.org/journal/jn (073.194.068.111) on October 11, 2020.

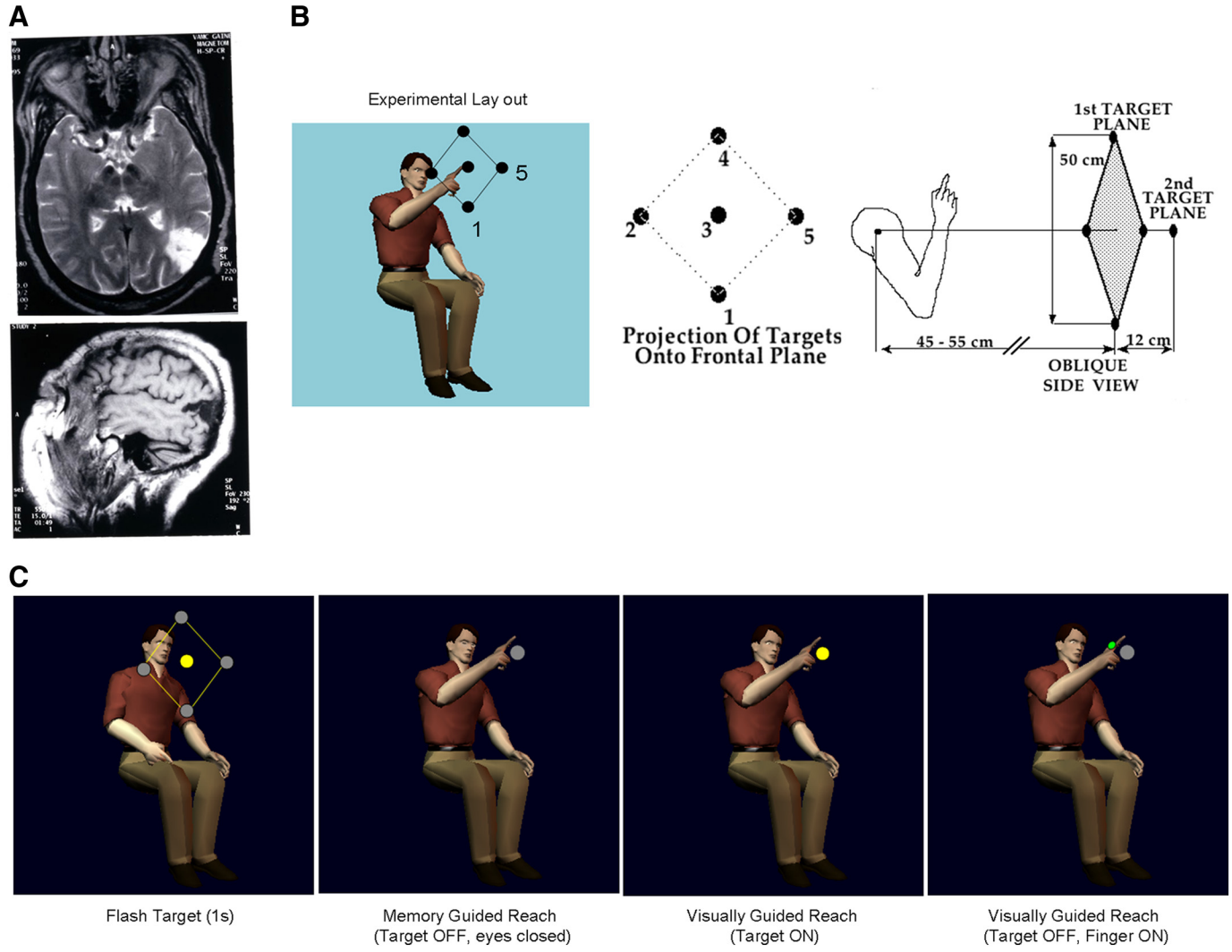

FIG. 2. *A*: a transverse T2 proton-weighted axial scan (*top*) and a sagittal T1 MRI scan (*bottom*). Following radiology conventions, the left side of the brain is shown on the right side of the figure. *B*: experimental layout representing a subject comfortably seating and reaching to one of the targets. Configuration and distances (cm) of the targets with a schematic diagram of the subject's arm in the initial position with the 5 targets in a slightly rotated side view. *C*: experimental conditions: a target is flashed at random in the dark and the subject is instructed to start from the posture in *B* and to reach in the dark in 1 of 3 conditions using a block design: memory, eyes closed-target OFF; extra-personal visual guidance, target ON throughout the reach; egocentric visual guidance, target OFF but moving finger-light ON.

3) Target (vision of target). The LED on the forefinger was off and thus the moving hand was not visible; however, the target light remained on and the participant's eyes remained open. Thus the subject saw the target but did not see either forefinger LED or the environment. The intensity of the target LED on the robot arm was adjusted to prevent the possibility of the subject seeing his finger at a distance >1–2 cm from the target. A strong overhead light was turned on between trials to prevent dark adaptation. In this target condition, the only available visual information throughout the movement was the point-light target.

There were 7 trials per target, with five target lights, for a total of 35 trials in each condition; however, in some trails, because of occlusion of the markers, 1 or 2 trials had to be dropped. The minimum number of trials per target in such rare cases was five. We found that wrist rotations in this paradigm can create marker occlusions and thus asked subjects not to move their wrist.

Ethics

All procedures with the human subjects were undertaken with the understanding and written consent of each subject. The Rutgers University Institutional Review Board approved the study. The study conforms to The Code of Ethics of the World Medical Association (Declaration of Helsinki).

Statistical and analytical measures

LANDMARKS OF TEMPORAL DYNAMICS IN RELATION TO SENSORY SPATIAL TRANSFORMATIONS. We systematically measured across space different critical temporal-dynamic points along the motion trajectories. These included the percent of total movement time to reach the maximum magnitude of the acceleration and the maximum magnitude of the velocity. Notice that we used the magnitudes (under Euclidean norm) of the vectors, and as such, these are positive scalars. We were not as interested in the shape of the speed profiles per se, because this aspect of the reach has been previously examined in detail by others (Abend et al. 1982; Lacquaniti and Soechting 1982; Lacquaniti et al. 1987; Morasso and Mussa Ivaldi 1982; Soechting and Lacquaniti 1981; Soechting et al. 1986).

We addressed instead when at a millisecond time scale the critical points of the speed and acceleration were reached relative to each

Downloaded from journals.physiology.org/journal/jn (073.194.068.111) on October 11, 2020.

other. Thus we focused on the frequency, spread, and centers of the distributions of the different temporal scales for acceleration and speed maxima. We examined first how these temporal parameters normally manifested across trials and conditions. Then we compared the normal performance to that of the left PPC patient. We used ANOVA with three conditions (dark, target, and finger conditions) and the percent of time to peak acceleration and that to peak velocity as the dependent variables.

DEFINITIONS: MOTION SEGMENTS, DELTA AND TAU. Since the patients' reaches had multiple velocity peaks, we examined those of first significance—>10 cm/s—and their corresponding acceleration peaks. We refer to acceleration $\|\vec{a}\|$ and speed $\|\vec{v}\|$ scalar quantities as the positive magnitudes of the acceleration and velocity vectors, respectively, and measure the times (in ms) at which their maximal values are achieved in each trajectory. We then study the frequency, centers, and spreads of these distributions and how they may be affected by the manipulations in the source of visual guidance.

A motion segment here is defined as one portion of the movement bounded between speed values rising above and falling toward 10 cm/s. This quantity was set based on the overall speed values of the normal controls and of the patient generally ranging from 1 to 250 cm/s in this task. Movement onset was defined as the point in time at which hand speed increased above 1 cm/s. The movement ended with a brief pause at the target location so we set the offset criterion at 0.5 cm/s. We also studied the accumulated distance traveled by the hand along the motion path up to the peak velocity (denoted delta cm) and the time length spent to travel that distance (denoted tau ms).

GEOMETRIC INVARIANTS. We used an index of multimodal sensory transformation and integration. The transformation part refers to the conversion of desired visual goals to adequate postural configurations to attain those goals. The integration part refers to the alignment and linear summation of multimodal sensory inputs. Normally angular displacements from joint rotations continuously map linearly to hand translational displacements (Fig. 1*C*) (Torres and Zipser 2002, 2004). Their rate of change has to preserve the smoothness and differentiability under transformation for the proper integration of the motion paths in both spaces. Our trajectory index measures the extent to which the patient's performance failed to preserve these relations compared with normal controls (Torres 2010).

We measured two ratios based on area and perimeter quantities obtained from the hand paths in various tasks. The initial and final location of each hand trajectory was joined by a straight line. The trajectories were resampled to obtain a fine temporal partition at 100 equally spaced points without distorting the spatial path. This was necessary for numerical integration to compute the area ratio explained below and to treat the curve as a geometric object independent of the temporal profile. Points in the path were projected onto the Euclidean straight line and the normal distance from the curve to the line measured. The point of maximum normal distance (maximum bending) was thus determined (Fig. 3*A*).

In Fig. 3*B,* the area ratio was defined as the quotient between the partial area A^{Partial} under the curve up to the point of maximum bending (highlighted in yellow) and the total area A^{Total}, $A = A^{\text{Partial}} / A^{\text{Total}}$. The perimeter ratio was defined in Fig. 3*B* as the quotient between the partial perimeter—the sum of the path length (X^{Partial}) up to the point of maximum bending, the length of the straight line connecting the initial hand position and the target up to the point of maximum bending (Y^{Partial}), and the segment measuring the bending distance at a right angle (Z)—and the total perimeter given by the total sum of the lengths of the hand path (X^{Total}) and the initial hand position to target straight line (Y^{Total}), $P = P^{\text{Partial}} / P^{\text{Total}} = X^{\text{Partial}} + Y^{\text{Partial}} + Z / (X^{\text{Total}} + Y^{\text{Total}})$ all segments depicted in Fig. 3*B*.

RATIO STATISTICS. The difference in variance between the area and the perimeter ratios is tied to the stability of the initiation of the movement. The end effector displacements in this segment of the reach affect the tempo and enter in the numerator term of both ratios. The Friedman test (Zar 1996) was used to analyze the difference between *patient T.R.* and controls in the variance between the area and the perimeter ratios, pooled across targets and trials.

TRAJECTORY BENDING EARLY AND LATE IN THE MOVEMENT. Bending was measured by projecting each trajectory onto the Euclidean straight line joining the initial position of the hand and the target (Fig. 3*A*). The normal distance (in cm) at each point of the motion was obtained. We quantified the possible effects of variable sensory-motor feedback availability on the path curvature across conditions. To this end, all the trajectories were divided into an early (1st 200 ms) and a late (last 300 ms) portion (Fig. 3*B*). The maximum bending was obtained in each of the early and late segments. The late portion of the path also provides information on spatial accuracy. ANOVAs were performed on this bending quantity. If the early bending was unaffected by these different experimental conditions in the normal system, we could assume that this portion of the reach was not under any kind of cognitive control. If, on the other hand, the manipulation of visual feedback selectively affected this early segment of the reach in the normal system, it would be valuable to examine how the compromised brain acted when the given visual cues anchored to the external world or to the body.

TRAJECTORY SKEWNESS. When blindfolded patients with hemispatial neglect attempt to fully extend their arm and point to their midsagittal plane, they often deviate toward ipsi-lesional space (Heilman et al. 1983). We developed a new measure of hemispatial neglect to quantify whether *patient T.R.*'s hand trajectories were skewed to the left or to the right side of 3D space. To construct this measure, we used the bending parameter described above. Each hand trajectory was resampled to have 50 equally spaced points, and each point in the path was projected onto the straight line connecting the initial hand and the target positions. At each point along this straight line, a circumference of radius equal to the degree of bending quantity was traced (Fig. 3*D*). At each circle, the corresponding point along the path was located in one of four quadrants (Fig. 3*E*). A point that fell in quadrants 1 and 4 was on the right side of space. A point that fell on quadrants 2 and 3 was on the left side of space. The distribution of this parameter on the circle was built using all points in all hand trajectories to all targets to address the issue of possible neglect of contralesional right hemispace in *patien T.R.*'s reaches.

RESULTS

In normal controls, the source of visual guidance scales the motion tempo but leaves the overall structure intact

In normal controls, the percent of time to reach the maximum acceleration α across all subjects and all trials pooled across all targets showed a nonunimodal distribution (significant according to the Hartigan's dip test, dip = 0.03, $P < 0.001$). A mixture of Gaussians fit yielded 40% of trials, where on average the maximum acceleration was reached at 68% of the total movement time (after the maximum speed), and 60% of the trials reached the maximum acceleration at 32% of the total movement time (before the maximum speed; Figs. 4 and 5). The first mode grouped the trials in which the acceleration had maximum magnitude in the acceleration phase of the reach (max acceleration time mode). The second mode grouped trials in which the magnitude of the acceleration was maximal in the deceleration phase of the reach (max deceleration time mode). Notice that it is expected to have two modes because of the shape of the instantaneous acceleration profile. Notice also that the maximum absolute magni-

Downloaded from journals.physiology.org/journal/jn (073.194.068.111) on October 11, 2020.

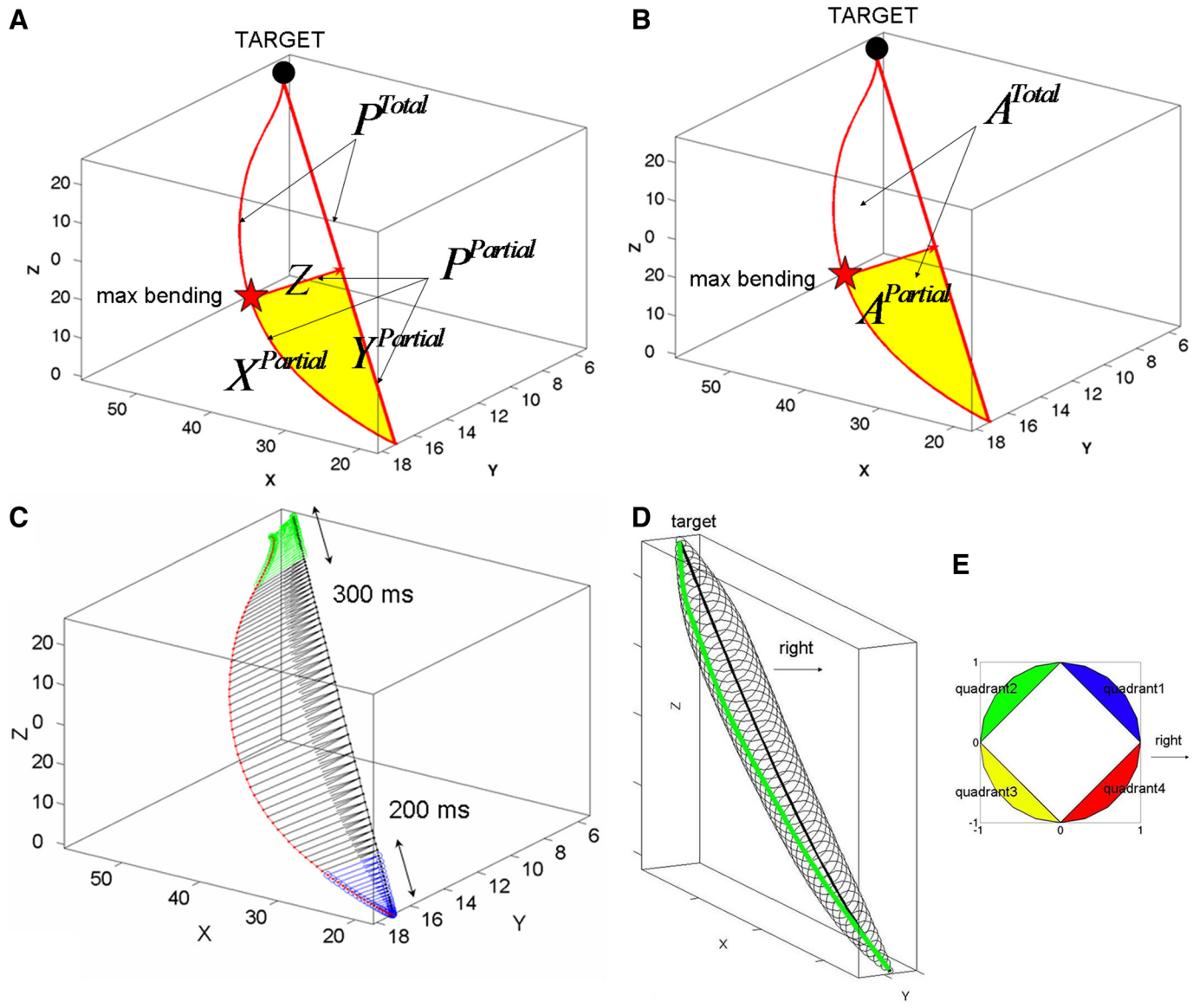

FIG. 3. Trajectory measures. *A*: partial perimeter (enclosing the shaded area) and defined by 3 segments in a typical hand trajectory from a normal subject. Star marks the point of maximum bending in relation to the Euclidean straight line used to define the 3 segments, *Z* (maximum normal distance from the curve to the line), X^{Partial} is the distance accumulated by the hand up to the point of maximum bending, and Y^{Partial} is the corresponding distance when projecting at a right angle onto the straight line. *B*: area ratio defined by dividing the partial area enclosed in yellow (up to the point of maximum bending) by the total area enclosed between the line and the curve spanned by the hand motion trajectory. *C*: hand motion trajectory (curved) bending in centimeters computed relative to the straight line joining the starting location and the target. The 1st 200 ms are marked. The last 300 ms are also marked. *D*: hand trajectory skewness measure: Sample motion hand path measured from a normal subject. Each hand trajectory was resampled (50 points) and projected onto the straight line. The normal distance from the line to the curve was obtained and used as the circumference radius at each point along the straight line. The hand path points fell on 1 of the sides of the circle. *E*: the circle was divided into 4 quadrants. Quadrants 1 and 4 were on the right side of space. Quadrants 2 and 3 were on the left side of space.

tude of acceleration was similar in both the acceleration and the deceleration modes. However, the time at which the maximum was attained in relation to the time at which the speed maximum was attained changed as a function of the source of sensory input.

Across trials, the center, spread, and height of these two modes provided important information because they were sensitive to the source of sensory input. Normally, the controls periodically alternated between these two modes from trial to trial, with higher variance in the temporal deceleration mode and higher frequency in the temporal acceleration mode (2-tailed *t*-test at 1% significance). In contrast, the performance of *patient T.R.* had a unimodal distribution (failed the Hartigan's test of bimodality, dip = 0.02, $P = 0.85$) of the percent of movement time to peak acceleration. A χ^2 goodness of fit test rejected the null hypothesis of a normal distribution ($P < 10^{-8}$, χ^2 statistics 46.34). His trial distribution was instead well fitted by a Gamma distribution (shape parameter 2.65 with [2.06 3.40] 95% CIs, and scale parameter 0.08 with [0.07 0.13] 95% CIs from maximum likelihood estimates).These distributions from typical speed performance in Fig. 4 are shown on the *top rows* of Fig. 5 for the controls (*A*) and for *patient T.R.* (*B*).

Downloaded from journals.physiology.org/journal/jn (073.194.068.111) on October 11, 2020.

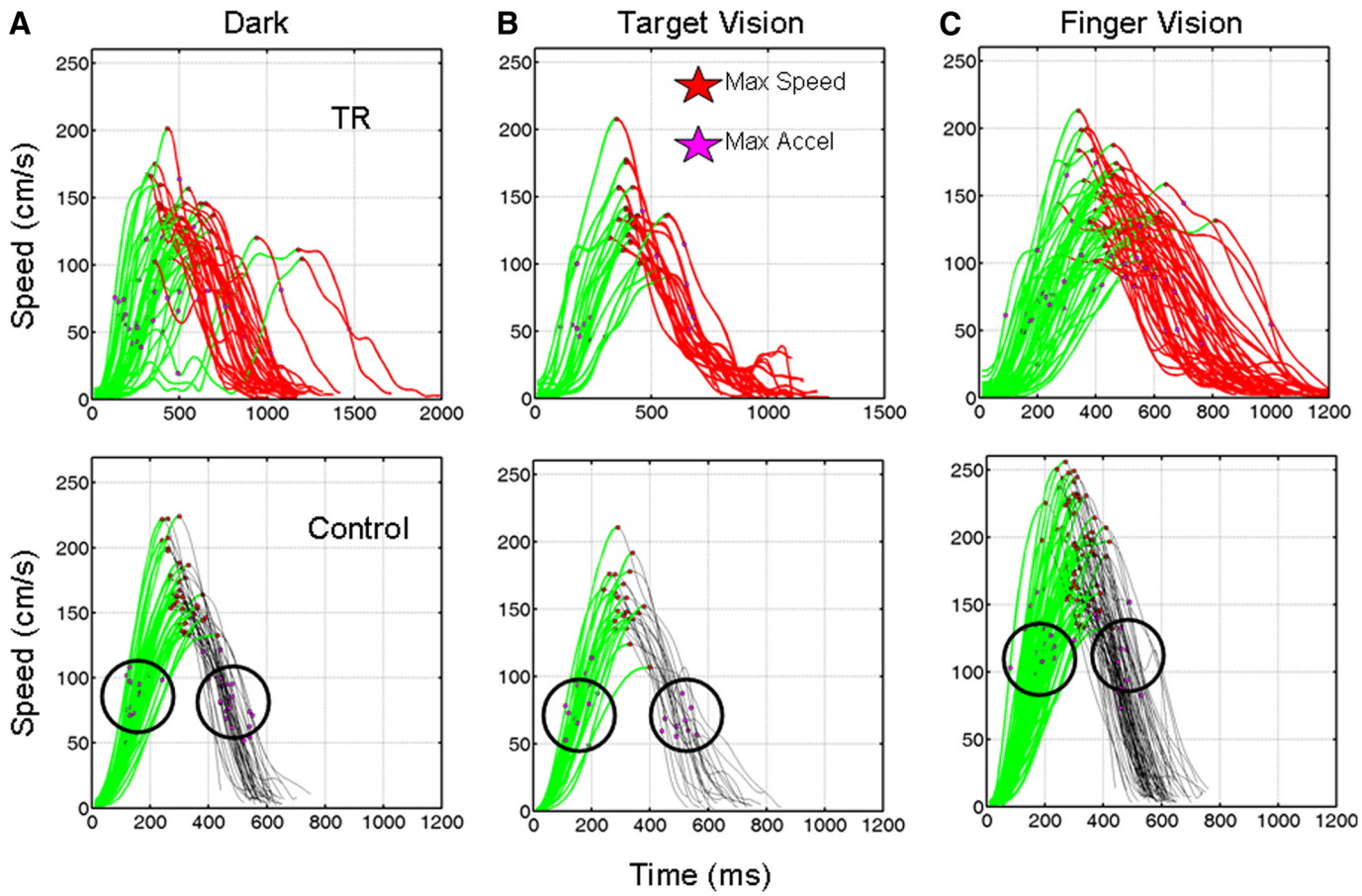

FIG. 4. Effects of the source of visual guidance on the hand speed (red patient, black representative normal control, green marks motion up to the time of maximum speed, red stars mark time of the maximum magnitude of the velocity vector, magenta stars mark the time of maximum magnitude of the acceleration vector, trajectories are to the central target location). *A*: dark condition: speed profiles of *patient T.R.* had multiple start-stop phases during the initiation of the reach, with a concentration of the maximum magnitude of the acceleration in the initial phase of the motion. In contrast, normal control had a smooth timing during the initial part of the reach with a bimodal distribution of the percent of time (α) to reach maximum acceleration. In some trials, this time occurred prior to the maximum speed, whereas in others, the maximum acceleration occurred after the maximum speed. Circles mark the points in time where this temporal dynamics landmark occurred. *B*: target vision: *patient T.R.* improved speed profiles. Initial timing became smoother and overall speed acquired normal speed range. The time to peak velocity (τ) became consistent and trials distributed as in normal controls according to the α. *C*: finger vision: normal control moved significantly faster in this condition compared with the other conditions (speed maximum dependent variable, 1-way ANOVA, $P < 0.01$). *Patient T.R.* took significantly longer to complete the reach despite higher speed maximum than in the other 2 conditions. TR motions were jerky both during the acceleration and the deceleration phases of the reach in contrast to the normal controls.

In the normal controls, the percent of movement duration to reach the speed maximum was uniformly distributed across all trials pooled across all targets, and subjects with the mean centered on 46% percent and nearly symmetric (bell shaped) speed profiles. This is shown in the *bottom panel* of Fig. 4*A*. ANOVA on the averaged percent of time to reach the maximum speed yielded a significant effect of the type of source of visual guidance across normal controls. This effect was significant at the 0.01 α level. This is shown in Fig. 6, whereas Fig. 4 compares the speed profiles of a typical subject to those of *patient T.R.* in each condition.

Abnormal temporal dynamics in patient T.R.

Patient T.R. had a significantly nonunimodal distribution (Hartigan's dip = 0.15, $P < 0.0001$) of the percent of movement time to reach the maximum speed. His two trial classes were best fitted by a mixture of two gamma distributions. In one class composed of fewer trials, the hand showed a peak velocity quite late in the motion, at 90% of the movement (shape 106.6 with [73.1, 161.3] 95% CIs, and scale 0.08 with [0.005, 0.012] 95% CIs). These were trials primarily from the finger vision case with an abnormally long acceleration phase and a speed profile with the maximum skewed to the right. In the other class, the hand reached the peak velocity abnormally early within 10% of the movement (shape 0.64 with [0.47, 0.86] 95% CIs, and scale 0.1 with [0.06 0.17] 95% CIs). Most trials in this distribution class came from the dark condition where the hand had an abnormally short acceleration phase and unstable initial timing. The distributions of these temporal landmarks are shown in the *bottom panels* of Fig. 5, *A* (controls) and *B* (*patient T.R.*).

Figure 4 highlights the point in time where the hand reached the maximum acceleration (circled in the normal controls). Whereas the normal controls had a nonunimodal distribution of this parameter in each target and for the pooled data across all targets and repeats, *patient T.R.*'s distribution was best fitted by a gamma. We performed a nonparametric ANOVA (Kruskal-Wallis test) and found statistically significant effects of the source of visual guidance on this parameter, particularly between the dark and target conditions. This is shown in Fig. 6*B* for *patient T.R.*

Downloaded from journals.physiology.org/journal/jn (073.194.068.111) on October 11, 2020.

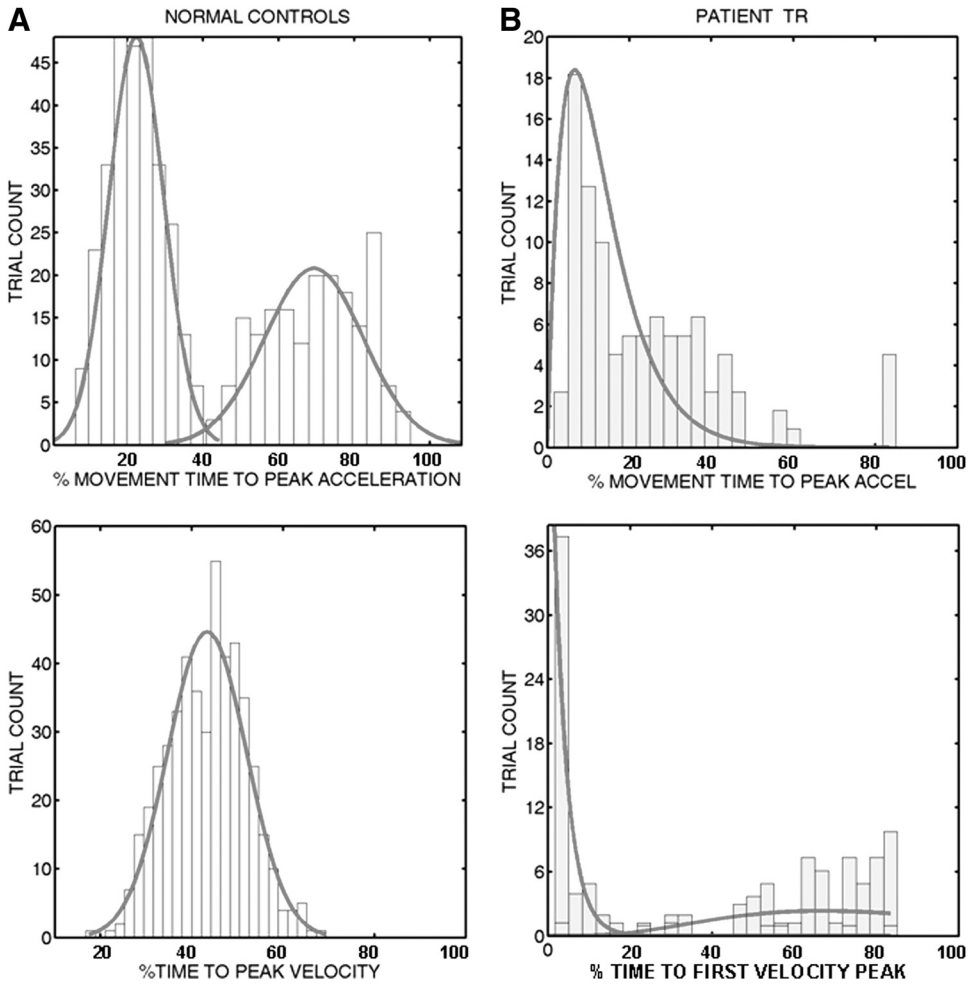

FIG. 5. Temporal dynamics landmarks along the hand trajectories. *A*: the percent of movement duration to reach the peak acceleration had a nonunimodal temporal distribution in the normal controls (all trials pooled across targets, subjects and repeats). The normal system moves with accelerations that peak at different time scales (in ms) despite similar magnitudes (cm/ms^2) at the maximum. The percent of time to peak velocity showed a normal unimodal distribution centered at 46% of the movement duration with mostly symmetric profiles across subjects and targets. The two modes of time to maximally accelerate or decelerate were present in all 5 targets. Across random target presentations, the hand periodically alternated between the 2 acceleration and deceleration modes with different frequency (height) and spread. Significantly larger variability (2-tail *t*-test at 1% significance) was observed in the time to decelerate maximally with a larger temporal distance from the peak velocity. *B*: abnormal unimodal distribution of the maximum acceleration time scale in *patient T.R.* A gamma distribution fitted best the patient data across all targets and repeats, whereby the hand reached the maximum magnitude of the acceleration earlier in time, in the initial portion of the reach in most trials. A χ^2 goodness of fit test rejected the null hypothesis of a normal distribution ($P < 10^{-8}$, χ^2 statistics 46.34). The percent of time to his 1st significant peak velocity (>10 cm/s) distributed in a nonunimodal fashion nonuniformly with a best maximum likelihood fitting of a mixture of 2 gammas (plotted in red). Notice that the patient's histogram quantifies the percent of time to reach the 1st significant velocity peak (as each motion trial had many peaks) above 10 cm/s. Trials where the hand reached the maximum speed toward the end of the reach had an abnormally long acceleration phase. These trials were primarily from the finger vision condition. Trials with maximum speed skewed toward the earlier portions of the reach came primarily from the dark condition under memory guidance.

Reach initiation and ending improved in patient T.R. with extrapersonal (target) visual guidance

In all conditions, normal subjects showed typical pointing trajectories with a smooth initiation phase. Their hand regularly started to slow down at about one half of the path length to the targets. In contrast, *patient T.R.*'s hand initiated the reach nonsmoothly and traveled highly variable cumulative distances at variable lengths of times (Figs. 4, *A* and *C*, 5*B*, and 7; Table 1). His speed profiles were particularly jerky in the conditions where the target was not visible during movement (Fig. 4, *A* and *C*). With continuous vision of the extrapersonal target, the distance δ became highly consistent and τ regained stability (Figs. 4*B* and 7*E*), regaining a smooth first segment of the reach as the normal controls had manifested.

Endpoint distance errors measured in Cartesian coordinates were obtained between the target position presented by the robot and the hand position at the end of the forward reach. This metric showed a similar pattern as the other metrics above: extrapersonal visual guidance improved endpoint accuracy to normal levels in the patient (5.31 cm in the patient vs. 5.47 cm in the control), with no significant differences according to the two-way ANOVA (target location and subject type as the 2 factors and endpoint error as the dependent variable; α level 0.01). In all conditions, there was normally a significant effect of target location.

Continuous vision of the target improved the patient's endpoint accuracy significantly in relation to both the no-vision and the finger vision cases. However, vision of the moving finger significantly worsened *patient T.R.*'s endpoint accuracy. In contrast, normal controls improved endpoint accuracy when the sensory

Downloaded from journals.physiology.org/journal/jn (073.194.068.111) on October 11, 2020.

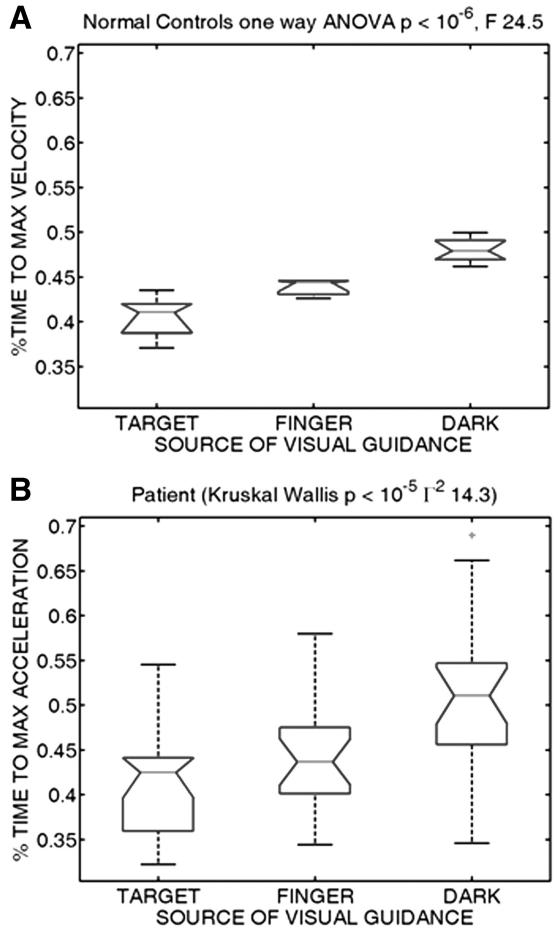

FIG. 6. Effects of the source of visual guidance on temporal dynamics landmarks. *A*: normal controls had a statistically significant effect of the source of visual guidance on the average percent ($100 \times [0, 1]$) of movement time to reach the maximum velocity along the hand motion trajectory, according to a 1-way ANOVA ($\alpha = 0.01$, $P < 10^{-6}$, $F = 24.5$ with 2 and 18° of freedom from 3 conditions and 9 subjects). *B*: *patient T.R.* had an effect of the source of visual guidance on the percent of time to maximum acceleration ($100 \times [0, 1]$; statistically significant between target and dark conditions) according to the nonparametric 1-way ANOVA (Kruskal Wallis test, $P < 10^{-5}$, $r^2 = 14.3$ with 2 and 72 degrees of freedom from 3 conditions and 25 trial per condition).

guidance was egocentric during the finger vision condition, a result congruent with endpoint spherical coordinates analysis of a data set from normal (Adamovich et al. 1998).

Geometric symmetry was violated with eyes closed by patient T.R. but restored under visual supervision with target vision

Normal controls conserved the hand trajectories geometric ratios despite the changes in temporal dynamics landmarks and the effects of the source of visual guidance. In the case of the percent of time to reach the peak acceleration, the distribution was significantly nonunimodal. In the case of the percent of time to reach the peak velocity, there was a significant effect of the source of visual guidance, and yet the symmetry (distribution center at one-half value) and the covariation of these ratios were maintained across conditions. This is shown in Fig. 7, *G* and *H*, in black. According to a Friedman's test (Zar 1996), the area and perimeter ratios were similar in normal subjects ($p = 0.8; \chi^2_{df=2.124} \leq 0.48, meanranks\ [8.1, 7.91, 7.93]$).

In contrast, these ratios were different from one half in *patient T.R.*, and they did not covary according to the Friedman's test. They were significantly different between each normal subject and *patient T.R.* ($p = 0; 39.4 \leq \chi^2_{df=1.6} \leq 47.7, meanranks\ [3.0, 7.98]$). *Patient T.R.* shifted the perimeter ratio distribution to a value significantly higher than 0.5 (*t*-test, $P < 0.01$). The system's unexpectedly long initial path length appeared to have upset its own inference of the stopping time. In the absence of visual feedback from the external target, his speed profiles had multiple velocity peaks indicating multiple slow-down-start-up phases unusual in automatic motions. This is shown in red in the Fig. 7, *A* and *C,* for *patient T.R.* Unlike in the case of normal controls, *patient T.R.*'s motion trajectories were not well characterized by a family of geodesics conserved under transformation from posture to hand spaces. This was confirmed by the study of his joint angle rotations, particularly those at the shoulder, which we recovered from the positional markers. The excursions of the unit vector representing the angular velocity were projected to the unit sphere, and their paths in the case of the normal controls were close to the great circles of the sphere (Fig. 8, normal), yet *patient T.R.*'s projections were erratic for the dark and finger conditions. In the case of extrapersonal visual guidance from the target light, *patient T.R.* regained the normality of the shoulder joint angular velocities. This is shown in Fig. 8 for the target vision case.

Paired to these aberrant joint angle velocity excursions in *patient T.R.* was an abnormally variable τ in the dark in the absence of extrapersonal cues (2-tailed pairwise *t*-test, $P < 0.01$; Fig. 7*D*) and also with finger vision. This was particularly so for the central target in depth located at the shoulder level, at the origin of the arm reference system. The faulty transformation between hand and arm paths (Fig. 8) caused excess endpoint trajectory bending that affected the perimeter (length) component, tilted the regression slope, and broke the symmetry and the ratio's covariation.

TABLE 1.

	Normal			TR		
Targets	No Vision τ, ms/δ, cm	Target Vision τ, ms/δ, cm	Finger Vision τ, ms/δ, cm	No Vision τ, ms/δ, cm	Target Vision τ, ms/δ, cm	Finger Vision $\delta\tau$, ms/δ, cm
Down 1	504 ± 95/29 ± 5	525 ± 48/25 ± 3	440 ± 120/22 ± 9	661 ± 217/35 ± 10	365 ± 36/22 ± 5	490 ± 204/33 ± 15
Left 2	444 ± 72/25 ± 5	485 ± 49/22 ± 2	428 ± 81/19 ± 6	590 ± 177/27 ± 5	507 ± 59/20 ± 3	416 ± 178/21 ± 9
Center 3	399 ± 78/21 ± 4	480 ± 70/26 ± 2	389 ± 61/26 ± 15	610 ± 293/35 ± 7	390 ± 21/24 ± 4	378 ± 198/27 ± 16
Up 4	448 ± 119/28 ± 7	435 ± 45/24 ± 2	425 ± 67/28 ± 12	488 ± 116/31 ± 9	427 ± 15/23 ± 1	425 ± 167/30 ± 13
Right 5	488 ± 85/30 ± 11	496 ± 66/26 ± 2	445 ± 111/33 ± 7	417 ± 98/31 ± 9	432 ± 26/23 ± 5	413 ± 56/35 ± 5

Downloaded from journals.physiology.org/journal/jn (073.194.068.111) on October 11, 2020.

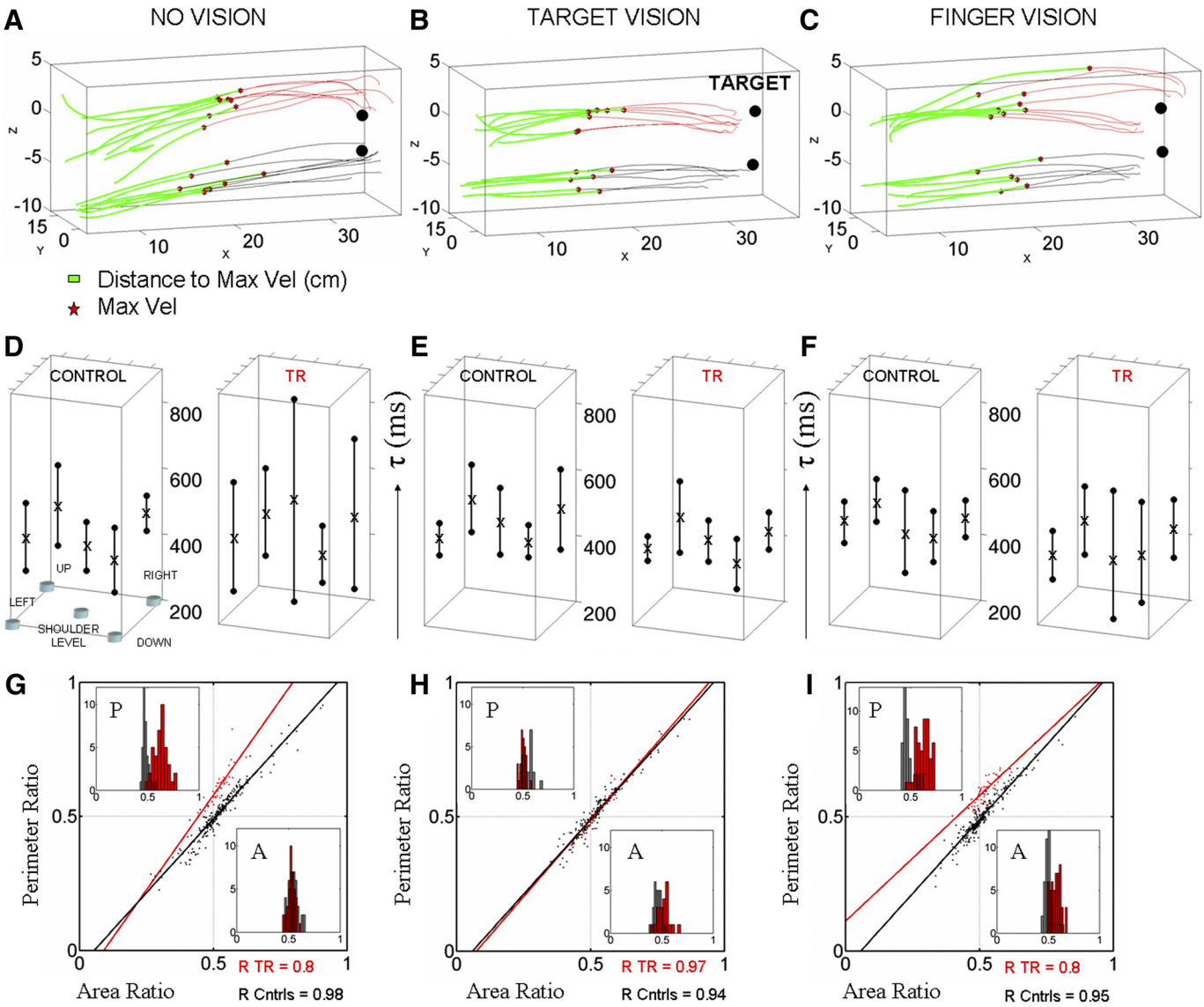

FIG. 7. Extrapersonal cue was sufficient to visually reconstruct the spatial map of τ and to voluntarily restore the geometric symmetry. *A–C*: hand trajectories of *patient T.R.* (red) and control (black) to the center target at shoulder level in the 3 conditions. Green highlights the cumulative distance traveled during the 1st acceleration phase (cm). Stars are the point on the curve where the velocity peak was reached. *D*: mean τ per target ± SD. Stability of τ breaks down in *patient T.R. E*: the extrapersonal cue brought the variability back to its normal range in each location. *F*: the egocentric cue did not help the patient. *G*: *patient T.R.* (red) broke the area-perimeter symmetry in the no-vision condition. *H*: the invariant geometric ratios ware repaired when τ became stable under visual feedback of the external target. *I*: vision of his moving finger worsened *patient T.R.*'s performance, so the ratio (red) broke down. The slope and intercepts were ([1.11,−0.06], [1.10,−0.05],[1.12,−0.07])for no vision, target vision, and finger vision, respectively, in normal subjects, with *R* values of 97, 98, and 95, respectively. *Patient T.R.*'s intercepts were ([1.48,−0.15], [1.09,−0.05],[0.83,0.10]), with *R* values of 82, 94, and 80, respectively.

When visual feedback of the target location was provided throughout the motion, *patient T.R.* performed at normal levels. The difference between the ratios was negligible ($p \leq 0.85$; $0.5 \leq \chi^2_{df=1.6} \leq 1.8$, *meanranks* [5.49, 5.50]) and, as in the normal controls, the value was close to 0.5 (2-tailed *t*-test, $P < 0.01$). *Patient T.R.*'s system recovered its performance with vision of the target. The stability of the initial timing could be repaired retinotopically from extrapersonal cues rather than from the integration of finger vision and kinesthetic information. The distribution of τ across space regained stability in *patient T.R.*'s reaches when he was given vision of the target. This improvement manifested in the first impulse of the movement with a temporal structure comparable to that of the normal controls (Fig. 7, *E* and *H*) and straighter first 200-ms segments of the trajectories across space (Table 2).

In general, with target vision, the patient's hand described significantly straighter paths both early and late in the movement (Table 2) when sensory motor feedback availability may have differed. On regaining trajectory stability, the geometric symmetry of *patient T.R.*'s reaches also was comparable to that observed in the controls (Fig. 7*H*).

When *patient T.R.* had vision of his moving finger but not of the target, his performance deteriorated at many different levels (Figs. 7*I*), and in the case of the ratios, this deterioration was different from that of the dark condition (Fig. 7*G*). His aberrant joint angle excursions mapped to irregular hand trajectories during finger vision (Fig. 8, parietal case-finger vi-

Downloaded from journals.physiology.org/journal/jn (073.194.068.111) on October 11, 2020.

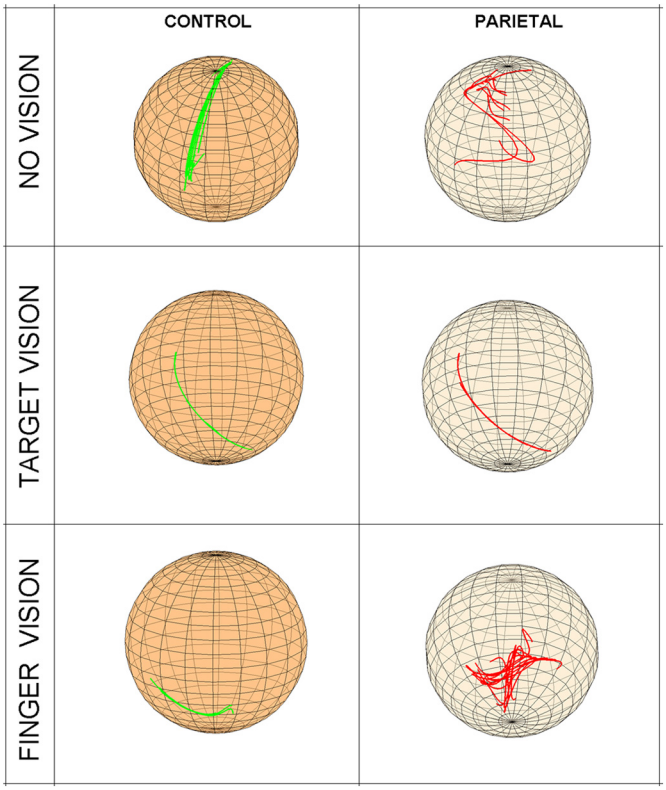

FIG. 8. Normalized shoulder joint angular velocity excursions to 1 target on the unit sphere. In the normal controls, case normalized angular velocity paths fall near a great circle on the unit sphere and the region changes as a function of the type of visual guidance. In *patient T.R.,* these joint angular excursions are erratic and noisy except when vision of the target is continuously available. (Spheres are rotated for better visualization. Joint angles were recovered from the positional sensors on the arm.) All paths from the motions to 1 target are superimposed.

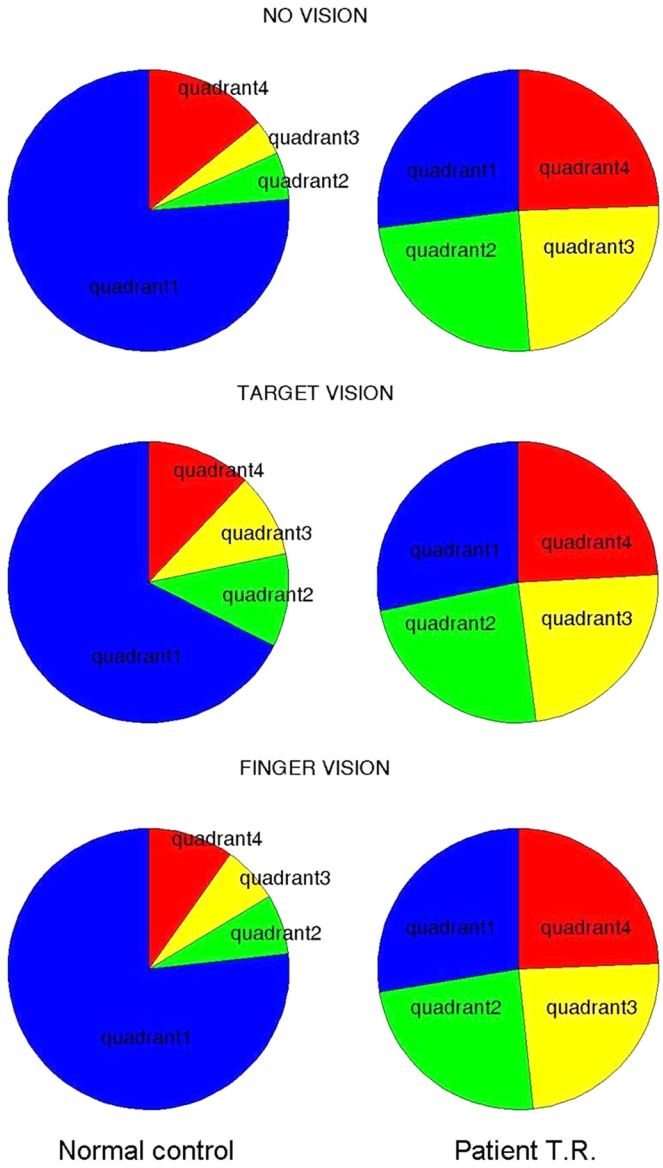

FIG. 9. Effect of the source of visual guidance on the hand trajectory skewness (normal controls vs. left posterior parietal cortex patient). Distribution of all points from all hand paths to all targets in the normal control compared with *patient T.R.* in each experimental condition. Notice that *patient T.R.* had hand path points also on quadrants 1 and 4 (on the right side of space affected by hemispatial neglect according to the line bisection test), but unlike in the normal control, this distribution was insensitive to the changes in the source of visual guidance.

sion; Fig. 7*C*). He had excess curvature in the hand trajectories both early and late (Table 2) and different ratios ($p = 0$; $39.9 \leq \chi^2_{df=1.6} \leq 47.73$, *meanrank* [*3, 8*]). Unlike in the dark case, where only the perimeter was affected, with finger vision, both the perimeter and the area ratios deviated significantly from 0.5 (*t*-test, $P < 0.01$). Whereas finger vision altered the hand path curvature significantly throughout the motion, vision of the target decreased trajectory bending both early and late in the movement (Table 2).

Spatial neglect of right hemispace in patient T.R. was invariant across experiments but his temporal (rate-of-change) deficit was not

Normal subjects had systematic biases to the right (Fig. 9, normals). In contrast, the patient did not exhibit this systematic bias to the right but moved toward left hemispace more frequently than did the control subjects, a finding that is consistent with the presence of right hemispatial neglect, as shown by the line bisection task (Fig. 9, patient). Furthermore, the analyses of spatial skewness of the hand trajectories showed the following.

1) *Patient T.R.*'s hand trajectories were not entirely skewed to the left as expected from his right hemispatial neglect

TABLE 2.

	Normal			*Patient T.R.*		
Averaged bending, cm	No Vision	Target Vision	Finger Vision	No Vision	Target Vision	Finger Vision
First 200 ms	7 ± 1.2	5 ± 1.8	2.2 ± 0.5	8 ± 3.8	2.3 ± 0.8	12 ± 4.8
Last 300 ms	8 ± 2.0	3 ± 0.8	2 ± 0.5	10 ± 2.5	2 ± 0.9	14 ± 4.5

Downloaded from journals.physiology.org/journal/jn (073.194.068.111) on October 11, 2020.

manifested in the line-bisection test. Oddly, his trajectory points were uniformly distributed in the left and the right sides of space (Fig. 9).

2) This measure of skewness signaling neglect in *patient T.R.* relative to the normal performance was insensitive to the experimental conditions. The distribution of trajectory points in space did not change in *patient T.R.* from one condition to another. The spatial deficit as measured by trajectory skewness had constancy in *patient T.R.*. This contrasted with his temporal deficit, which was highly sensitive to the experimental conditions and was repaired only when the visual cue was in extrapersonal space. It also contrasted with the distribution of endpoint errors, which was significantly different in the target vision condition.

3) The distribution in space of hand trajectory skewness in the normal controls changed with different sources of visual guidance (Fig. 9). In addition, the normal subjects manifested a strong rightward bias that *patient T.R.* did not have. This strong rightward bias was also manifested in the endpoint errors of the forward reach stroke.

DISCUSSION

This study addressed the possible effects of different sources of visual guidance on sensory-spatial transformations for reaching acts and the potential contribution of such transformations to the fluidity of the reach tempo. Specifically, we studied in normal controls and in a patient with left PPC injury the problem of aligning different forms of sensory input in the context of memory guided reaches, visually guided reaches from an extrapersonal source (a target in space), and reaches that were visually guided by the continuous motion of the subject's moving hand without target vision.

In the first part of this work, we studied how normal participants changed their reach tempo under manipulations of the source of visual guidance. We learned that, whereas the overall temporal structure of the reach was conserved, the time scales of acceleration and speed maxima along the hand motion trajectories significantly changed. These parameters of the motion were studied under a geometric framework that permitted the time-independent assessment of sensory-spatial transformation and integration processes in automated reaches. In automated motions, it had been difficult to separate kinematics and dynamics parameters as they normally covary. We designed a dynamics-invariant metric to dissociate deficits in temporal control and coordination from deficits in sensory transformation and integrations processes. We hypothesized that such processes could contribute to the fluidity of the reach tempo and found supporting evidence for this proposition. To assess our hypothesis, we used a new trajectory metric. This metric cannot possibly assess the control of movement timing—because it is a dynamics invariant metric (Torres 2010; Torres and Andersen 2006)—yet it can be used to evaluate multimodal sensory transformations deficits in the compromised system and their improvement toward normality under a specific source of sensory input.

In the second part of the study, we compared the performance of the normal controls to that of *patient T.R.*, the experimental participant who sustained an injury to his left PPC to learn *1*) whether the lesion disrupted the integration and alignment of different sensory-based displacements (angular and linear), thus impairing the proper scaling of hand speed and hand acceleration, and *2*) whether an extrapersonal source of visual guidance could compensate better for the unstable reach timing than egocentric visual guidance anchored on the moving hand or no visual guidance at all.

We surmised that, given the roles of the PPC in sensory-motor coordinate transformations, a lesion to this region (without impairments in the execution of the motor commands) could affect the alignments of the positional displacements and their interrelations in different sensory spaces. These possible disruptions would in turn affect the continuity of sensory integration along the motion path and alter the overall structure of the reach tempo.

To provide the formal means to evaluate these ideas, we first built a geometric model of different sensory-motor transformation scenarios (Torres 2010). Within a geometric theoretical framework, we studied sensory-motor transformations and sensory-motor integration issues independent of the motion dynamics. Using this framework we derived a time-invariant sensory-motor transformation/integration metric from the hand motion curves and tested this objective metric in the patient in relation to the normal controls for each visual guidance manipulation. In our previous use of this metric, we found that, whereas insensitive to striking changes in arm-reaching dynamics, the metric identified irregularities in the posture-to-hand transformation map. Specifically this metric quantifies failure in the coordinate transformation/map relating joint rotations and hand's translations. Their relative rates of change affect the timing (as other elements do—forces, torques, muscle fatigue, etc.), but when the source of visual guidance was external, both the rates of change of rotational displacements and hand translations improved in the patient, and this geometric measure captured that improvement independent of temporal modulations from sensory manipulations observed in normal controls. The metric does not explain anything at all about the control of timing. It could not possibly do so because it is a dynamics-invariant measure.

For control subjects, we found marked spatio-temporal changes with manipulations in the source of visual guidance. These were mainly scaling changes that did not affect the overall temporal structure of the reach. Despite the scaling changes in the reach tempo, these ratios held a strong pattern of similarity across randomly flashed target locations for each normal control subject. Such time-invariant patterns in the geometric ratios, however, were violated in the patient with left PPC damage and compensated toward normal performance only with continuous vision of the external target. *Patient T.R.*'s performance deteriorated with visual feedback from his moving finger—even more than when reaching for the target with eyes closed in complete darkness. These marked differences in reaching performance of the PPC patient in the two conditions (finger vision vs. no vision) were systematic despite the fact that, in both conditions, he had to rely on his visual memory of the target location. We studied this measure in patients with basal ganglia deficits who suffer from Parkinson's disease. (Torres et al. 2008). That work quantified different aspects of the timing (bradykinesia) and lack of coordination and identified a different source of visual guidance (vision of the moving finger rather than of the target) as the compensatory one.

Downloaded from journals.physiology.org/journal/jn (073.194.068.111) on October 11, 2020.

In *patient T.R.,* the various temporal dynamics landmarks under study were dramatically affected by the left PPC lesion. In particular, in the absence of continuous visual guidance from the external target, the initiation of his reach was erratic because his hand gained too much acceleration at the start of the reach, particularly in the finger vision condition where his initial speed was abnormally fast. In contrast, in the target vision condition, he showed significant improvements in the initial timing of the reach. In this block, he regained the apparent normal tendency of the arm-hand system to alternate from trial to trial between accelerating maximally when starting or when ending the reach. With target vision, his hand speed profiles also regained normality: a consistent timing to the velocity peak, a single speed maximum halfway to the target, and a smooth initial segment of the motion.

Normal controls showed two Gaussian distribution modes of the percent of movement time to reach the absolute maximum acceleration (α). Normally the hand periodically alternated between timing the peak acceleration in the acceleration phase or in the deceleration phase. In the normal controls, the height, spread, and center of these modes provided information about the different time scales of acceleration across different spatial target directions despite a uniform distribution of the absolute acceleration maximum with negligible differences in the maximum magnitude from trial to trial. Notably normal participants had more temporal variability when decelerating than when accelerating, and the centers, spread, and heights of the modes were sensitive to the source of sensory input. In contrast, *patient T.R.* showed a unimodal distribution of α best fitted by a gamma distribution. Across random repeats to various spatial locations, *patient T.R.* reached the absolute acceleration maximum mostly within 40% of the total movement duration. He also had multiple start-stop reach segments with multiple velocity peaks. Target vision corrected all of these chronological irregularities.

When continuously being able to view the target, *patient T.R.* also improved his joint angular velocity excursions. These continuous angular displacements aligned onto the desirable linear velocity displacement toward the target in the hand space. This sensory-spatial transformation improvement was also quantified by the symmetric trajectory ratios and their covariation. Only in the target vision condition did *patient T.R.* regain the level of normal performance quantified by this sensory-spatial transformation index.

The time invariance of the geometric trajectory ratios in the normal controls, their sensitivity to faulty sensory-spatial transformations in the presence of injury to the left PPC in *patient T.R.,* and the quantification of his improvements in the movement tempo with external visual guidance all point to a different new aspect of movement timing contributed by sensory-spatial transformations. There may be many other potential sources for the temporal deficits and improvements observed in the parietal patient, yet in this region, a specific source of visual input compensated best for such deficits, and a dynamics invariant metric could objectively quantify both the original deficits and the improvements. This suggests that the left PPC is one of many contributing areas to the fluidity of the reach tempo and invites a new area of inquiry regarding chronological aspects of the reach that may be tied to external visual input and proper sensory-spatial transformations. This role had not been previously quantified with an objective, time-invariant geometric index of reach performance.

ACKNOWLEDGMENTS

We thank O. Fookson, S. Adamovich, and M. Berkinblit for help in data collection and processing and Profs. Jerry Feldman from University of California Berkeley and Sandro Mussa-Ivaldi from Northwestern University for valuable comments and suggestions.

GRANTS

This work was supported in part by National Institute of Neurological Disorders and Stroke Grant 2 R01 NS-036449 to H. Poizner, National Science Foundation (NSF) Grant SBE-0542013 to the Temporal Dynamics of Learning Center, and NSF Cyber Enabled Discovery and Innovation Type I (Idea) type I Grant 0941587 to E. B. Torres.

DISCLOSURES

No conflicts of interest, financial or otherwise, are declared by the authors.

REFERENCES

Abend W, Bizzi E, Morasso P. Human arm trajectory formation. *Brain* 105: 331–348, 1982.

Adamovich SV, Berkinblit MB, Fookson O, Poizner H. Pointing in 3D space to remembered targets. I. Kinesthetic versus visual target presentation. *J Neurophysiol* 79: 2833–2846, 1998.

Altmann SL. *Rotations, Quaternions, and Double Groups.* New York: Clarendon Press, 1986.

Andersen RA. Encoding of intention and spatial location in the posterior parietal cortex. *Cereb Cortex* 5: 457–469, 1995.

Andersen RA, Snyder LH, Li CS, Stricanne B. Coordinate transformations in the representation of spatial information. *Curr Opin Neurobiol* 3: 171–176, 1993.

Andersen RA, Zipser D. The role of the posterior parietal cortex in coordinate transformations for visual-motor integration. *Can J Physiol Pharmacol* 66: 488–501, 1988.

Atkeson CG, Hollerbach JM. Kinematics features of unrestrained vertical arm movements. *J Neurosci* 5: 2318–2330, 1985.

Blangero A, Gaveau V, Luaute J, Rode G, Salemme R, Guinard M, Boisson D, Rossetti Y, Pisella L. A hand and a field effect in on-line motor control in unilateral optic ataxia. *Cortex* 44: 560–568, 2008.

Buneo CA, Batista AP, Jarvis MR, Andersen RA. Time-invariant reference frames for parietal reach activity. *Exp Brain Res* 188: 77–89, 2008.

Buneo CA, Jarvis MR, Batista AP, Andersen RA. Direct visuomotor transformations for reaching. *Nature* 416: 632–636, 2002.

Desmurget M, Epstein CM, Turner RS, Prablanc C, Alexander GE, Grafton ST. Role of the posterior parietal cortex in updating reaching movements to a visual target. *Nat Neurosci* 2: 563–567, 1999.

Desmurget M, Grafton S. Forward modeling allows feedback control for fast reaching movements. *Trends Cogn Sci* 4: 423–431, 2000.

Fujii N, Graybiel AM. Time-varying covariance of neural activities recorded in striatum and frontal cortex as monkeys perform sequential-saccade tasks. *Proc Natl Acad Sci USA* 102: 9032–9037, 2005.

Grea H, Pisella L, Rossetti Y, Desmurget M, Tilikete C, Grafton S, Prablanc C, Vighetto A. A lesion of the posterior parietal cortex disrupts on-line adjustments during aiming movements. *Neuropsychologia* 40: 2471–2480, 2002.

Heilman KM. Case reports and case studies, an endangered species. *Cogn Behav Neurol* 17: 121–123, 2004.

Heilman KM, Bowers D, Watson RT. Performance on hemispatial pointing task by patients with neglect syndrome. *Neurology* 33: 661–664, 1983.

Heilman KM, Valenstein E. *Clinical Neuropsychology.* New York: Oxford, 2003.

Heilman KM, Valenstein E (Editor). *Clinical Neuropsychology.* Oxford: Oxford, 2003.

Heilman KM, Watson RT. Mechanisms underlying the unilateral neglect syndrome. *Adv Neurol* 18: 93–106, 1977.

Heilman KM, Watson RT, Greer M. *Handbook for Differential Diagnosis of Neurologic Signs and Symptoms.* New York: Appleton-Century-Crofts, 1977.

Downloaded from journals.physiology.org/journal/jn (073.194.068.111) on October 11, 2020.

Jin DZ, Fujii N, Graybiel AM. Neural representation of time in cortico-basal ganglia circuits. *Proc Natl Acad Sci USA* 106: 19156–19161, 2009.

Kalaska JF, Cohen DA, Prud'homme M, Hyde ML. Parietal area 5 neuronal activity encodes movement kinematics, not movement dynamics. *Exp Brain Res* 80: 351–364, 1990.

Kalaska JF, Hyde ML. Area 4 and area 5: differences between the load direction-dependent discharge variability of cells during active postural fixation. *Exp Brain Res* 59: 197–202, 1985.

Kalaska JF, Scott SH, Cisek P, Sergio LE. Cortical control of reaching movements. *Curr Opin Neurobiol* 7: 849–859, 1997a.

Kertesz A. *Western Aphasia Battery.* New York: Gune and Stratton, 1982.

Khan AZ, Crawford JD, Blohm G, Urquizar C, Rossetti Y, Pisella L. Influence of initial hand and target position on reach errors in optic ataxic and normal subjects. *J Vis* 7: 1–16, 2007.

Khan AZ, Pisella L, Vighetto A, Cotton F, Luaute J, Boisson D, Salemme R, Crawford JD, Rossetti Y. Optic ataxia errors depend on remapped, not viewed, target location. *Nat Neurosci* 8: 418–420, 2005.

Krakauer JW, Ghilardi MF, Ghez C. Independent learning of internal models for kinematic and dynamic control of reaching. *Nat Neurosci* 2: 1026–1031, 1999.

Lacquaniti F, Ferrigno G, Pedotti A, Soechting JF, Terzuolo C. Changes in spatial scale in drawing and handwriting: kinematic contributions by proximal and distal joints. *J Neurosci* 7: 819–828, 1987.

Lacquaniti F, Soechting JF. Coordination of arm and wrist motion during a reaching task. *J Neurosci* 2: 399–408, 1982.

Morasso P, Mussa Ivaldi FA. Trajectory formation and handwriting: a computational model. *Biol Cybern* 45: 131–142, 1982.

Nishikawa KC, Murray ST, Flanders M. Do arm postures vary with the speed of reaching? *J Neurophysiol* 81: 2582–2586, 1999.

Pisella L, Grea H, Tilikete C, Vighetto A, Desmurget M, Rode G, Boisson D, Rossetti Y. An 'automatic pilot' for the hand in human posterior parietal cortex: toward reinterpreting optic ataxia. *Nat Neurosci* 3: 729–736, 2000.

Pisella L, Sergio L, Blangero A, Torchin H, Vighetto A, Rossetti Y. Optic ataxia and the function of the dorsal stream: contributions to perception and action. *Neuropsychologia* 47: 3033–3044, 2009.

Poizner H, Clark MA, Merians AS, Macauley B, Rothi LG, Heilman KM. Joint coordination deficits in limb apraxia. *Brain* 118: 227–242, 1995.

Poizner H, Mack L, Verfaellie M, Rothi LG, Heilman KM. Three-dimensional computergraphic analysis of apraxia. *Brain* 113: 85–101, 1990.

Poizner H, Merians AS, Clark MA, Macauley B, Rothi LJ, Heilman, KM. Left hemispheric specialization for learned skilled, and purposeful action. *Neuropsychology* 12: 163–182, 1998.

Riddoch MJ, Humphreys GW. *BORB: Birmingham Object Recognition Battery.* Hove, UK: Lawrence Erlbaum Associates, 1993.

Sainburg RL, Kalakanis D. Differences in control of limb dynamics during dominant and nondominant arm reaching. *J Neurophysiol* 83: 2661–2675, 2000.

Schaefer SY, Haaland KY, Sainburg RL. Disociation of initial trajectory and final position errors during visiomotor adaptation following unilateral stroke. *Brain Res* 17: 78–91, 2009.

Schmahmann JD. Disorders of the cerebellum: ataxia, dysmetria of thought, and the cerebellar cognitive affective syndrome. *J Neuropsychiatry Clin Neurosci* 16: 367–378, 2004.

Schmahmann JD, Weilburg JB, Sherman JC. The neuropsychiatry of the cerebellum - insights from the clinic. *Cerebellum* 6: 254–267, 2007.

Scott SH, Sergio LE, Kalaska JF. Reaching movements with similar hand paths but different arm orientations. II. Activity of individual cells in dorsal premotor cortex and parietal area 5. *J Neurophysiol* 78: 2413–2426, 1997.

Soechting JF. Effect of load perturbations on EMG activity and trajectories of pointing movements. *Brain Res* 451: 390–396, 1988.

Soechting JF, Lacquaniti F. Invariant characteristics of a pointing movement in man. *J Neurosci* 1: 710–720, 1981.

Soechting JF, Lacquaniti F, Terzuolo CA. Coordination of arm movements in three-dimensional space. Sensorimotor mapping during drawing movement. *Neuroscience* 17: 295–311, 1986.

Torres E, Andersen R. Space-time separation during obstacle-avoidance learning in monkeys. *J Neurophysiol* 96: 2613–2632, 2006.

Torres EB. New symmetry of intended curved reaches. *Behav Brain Functions* 6: 21, 2010.

Torres EB, Heilman KM, Poizner H. Complementary functions of the parietal lobe and basal ganglia in accurate reaching. *Soc Neurosci* 818, 2007.

Torres EB, Zipser D. Reaching to grasp with a multi-jointed arm. I. Computational model. *J Neurophysiol* 88: 2355–2367, 2002.

Torres EB, Zipser D. Simultaneous control of hand displacements and rotations in orientation-matching experiments. *J Appl Physiol* 96: 1978–1987, 2004.

Zar J. *Biostatistical Analysis.* Upper Saddle River, NJ: Prentice-Hall, 1996.

Zipser D, Andersen RA. A back-propagation programmed network that simulates response properties of a subset of posterior parietal neurons. *Nature* 331: 679–684, 1988.

Downloaded from journals.physiology.org/journal/jn (073.194.068.111) on October 11, 2020.